# Direct Probe of End-Segment Distribution in Tethered Polymer Chains

**J. K. Basu,[†,‡] J. C. Boulliard,[§] B. Capelle,[§] J. Daillant,[†] P. Guenoun,*[,†] J. W. Mays,[⊥] and J. Yang[#]**

*LIONS, Service de Chimie Moléculaire, CEA Saclay, F-91191 Gif sur Yvette, France; Department of Physics, Indian Institute of Science, Bangalore 560 012, India; Institut de Minéralogie et de Physique des Milieux Condensés, 140 rue de Lourmel, 75015 Paris, France; Department of Chemistry, University of Tennessee, Knoxville, Tennessee 37996; Chemical Sciences Division and Center for Nanophase Materials Sciences, Oak Ridge National Laboratory, Oak Ridge, Tennessee 37831; and Waters Corporation, 34 Maple Street, Milford, Massachusetts 01757*

*Received April 6, 2007; Revised Manuscript Received May 4, 2007*

ABSTRACT: End-tethered chains made of an adsorbed diblock copolymer of polystyrene (PS)−polyisoprene (PI) bearing an end-segment including a Ge atom are built by the Langmuir−Schaeffer technique. They are studied both in the dry state and in a good solvent for the PI chain using grazing incidence X-ray standing waves. The analysis of the signal provides a direct measurement of the end-segment distribution which is found to be singular and mostly localized to a plane in the dry case. In the good solvent case, end-segments are found to span the entire assembly and compare very well with results obtained by Kreer et al. [Kreer, T.; Metzger, S.; Müller, M.; Binder, K.; Baschnagel, J. *J. Chem. Phys.* **2004**, *120*, 4012].

## I. Introduction

End-tethered polymer layers are ubiquitous in various applications ranging from colloidal stabilization to modification of wetting, adhesive, or frictional properties of surfaces and interfaces at which they are anchored.

Polymer brushes refer to long-chain polymer molecules tethered by one end to a surface or interface by physical or chemical attachment. Brushes are obtained for sufficiently high tethering density so that chains are forced to stretch away from the interface, much further than the unperturbed bulk size of the chain, especially if placed in a good solvent for the chains.[1]

At lower densities, end-tethered chains are in the so-called "mushroom" regime where dimensions of the chains are not perturbed with respect to the bulk dimensions. This regime is practically more accessible than the brush regime since high grafting densities are quite often hard to achieve. The "mushroom" regime can also be more relevant in practice as it is easier to achieve and can impart interesting mechanical properties.[2]

The interfacial structure determines the nature and range of interaction between polymer surfaces. This emphasizes the necessity to get a detailed knowledge about the surface structure at the level of individual monomers. Despite the enormous complexity of having to predict the structure of the surface of a system composed of thousands of monomers, theory has been able, under some restrictive assumptions like those underlying the strong stretching theory (SST),[1,3,4] to predict both the density of segments and the distribution of the end-segments in a brush.[5] Whereas mean-field theories are reasonably accurate for weakly fluctuating brushes, less dense layers like mushrooms cannot be described in mean-field terms.[6] This has been done by renormalization group calculations, scaling theories, and numerical simulations.[7]

* Corresponding author. E-mail: patrick.guenoun@cea.fr.
† LIONS, Service de Chimie Moléculaire.
‡ Indian Institute of Science.
§ Institut de Minéralogie et de Physique des Milieux Condensés.
⊥ University of Tennessee and Oak Ridge National Laboratory.
# Waters Corporation.

Density profiles have been measured by neutron scattering[8] or neutron reflectivity for both neutral and charged chains.[9] It was suggested in one of the original papers by Milner et al.[4] that a good way to test the predictions of the SST would be to measure the end-segment density distribution by fluorescent labeling of the end of polymer chains. However, no direct experimental determination of this very important end-segment distribution exists so far.

On solid substrates, several methods have been proposed to build end-tethered polymer layers. By using end-functionalized polymers, polymer layers can be prepared on suitable substrates utilizing the specific interaction between the polymer end-group and the substrate by physisorption as well as by chemisorption.[10] Another convenient method of tethering chains is to use diblock copolymers. Specifically, if a highly asymmetric diblock copolymer is placed in a solvent selective to the larger block, the diblock copolymer can adsorb onto the substrate surface by the smaller block.[11] This occurs because of the tendency to minimize unfavorable interaction between the latter block and the solvent. We have specially designed a block copolymer of polystyrene−polyisoprene−Ge (PSPIGe) having one germanium (Ge) atom, chemically introduced, in the terminal PI monomer of each molecule, in order to determine the end-segment distribution. The block copolymers are then adsorbed onto specially prepared solid substrates (polystyrene-coated silicon) using a special horizontal transfer version of the standard Langmuir−Schaeffer technique: an organic solution of the copolymer is spread at the water surface, compressed at the required density, and then transferred to the substrate. The above process results in the grafting, to the underlying polystyrene layer, of the polystyrene block of PSPIGe, which then becomes irreversibly attached by annealing above the glass transition temperature of polystyrene[12] and subsequent quenching to room temperature.

The adsorbed block copolymer layer is investigated both in air and in a solvent (hexadecane), which is selectively good for the polyisoprene block, using the grazing incidence X-ray standing wave fluorescence (GIXSWF) technique. The experiments were performed at LURE, France, at an incident X-ray

10.1021/ma070817d CCC: $37.00 
Published on Web 07/28/2007

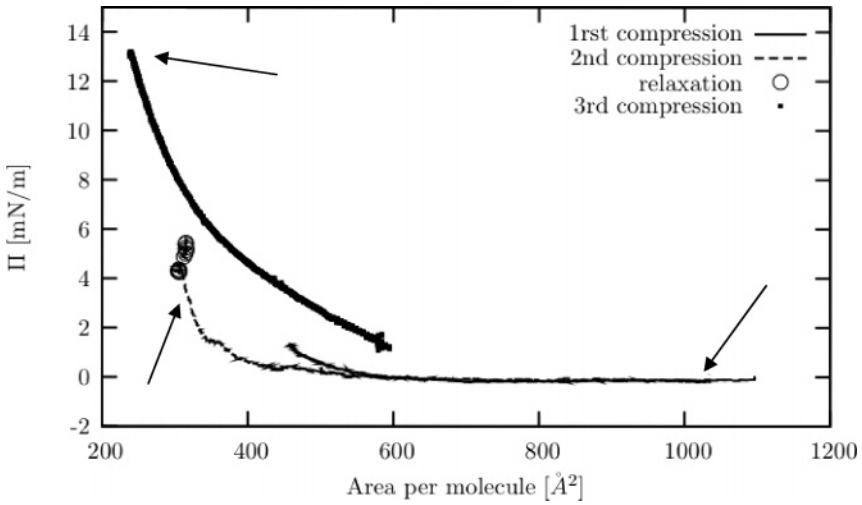


**Figure 1.** Successive compressions resulting in a complete isotherm of the polymer at the air−water interface. Second compression was made after addition of 100 $\mu$L to the initial 200 $\mu$L and the third compression after another addition of 100 $\mu$L. Arrows point to places where BAM images shown in Figure 2 were taken. Empty circles indicate a pressure relaxation (pressure rise with time) at a fixed area overnight (second compression).

energy of 12.795 keV to excite Ge K fluorescence. By using the standing waves generated above the surface of the substrate below its critical angle, this technique is shown to be able to sense the distribution of Ge atoms normal to the surface and hence the end-monomer distribution by virtue of the chemical labeling process of the end-monomers.

## II. Theoretical Background

Early work on brushes was based on both Flory-type mean-field arguments, due to Alexander,[3] and the simple scaling approach, due to de Gennes,[4] which predicted the scaling of the brush height, $h$, as

$$h = N(\sigma w)^{1/3} \tag{1}$$

where $N$ is the number of monomers in the chain and $\sigma$ is the surface density of chains while $w$ is the excluded volume parameter, which is related to the Flory−Huggins interaction parameter. The basic assumption in this approach is that the monomer density is homogeneous throughout the brush layer—implying a step function density profile—and that the chains behave identically with their ends strictly terminating at a distance $h$ from the grafting surface. Numerical calculations based on the self-consistent-field theoretical (SCFT) methods were also performed.[13] The numerical calculations confirm the above scaling relation (eq 1) but show that the monomer density profile is inhomogeneous and substantially different from that assumed by Alexander and de Gennes. In order to provide a greater physical insight, Milner et al.[5] and Zhulina et al.,[14] following calculations on block copolymer melts by Semenov,[15] performed an analytic SCFT calculation by making the simplifying assumption of a strongly stretched brush. Following the SST approximations,[16] the height $h$ vs the distance between chain $D$ reads as

$$h = \left(\frac{8}{\pi^2}\right)^{1/3} (\upsilon p)^{1/3} \left(\frac{a}{D}\right)^{2/3} Na \tag{2}$$

where $\upsilon = T - \theta/T$ with $\theta$ the theta temperature of the polymer and $p$ the ratio of the persistence length of the polymer to the monomer length.

In the mushroom case, scaling theory describes only a part (small $z$) of the monomer profile, but a renormalization group approach is necessary to obtain the full monomer distribution. Each chain occupies a half-sphere of a radius equal to the Flory radius in good solvent, $R_F = N^{\nu}a$ with $\nu$ the Flory exponent equal to 0.588 and where $a$ is the monomer size. Scaling arguments[17] lead to a monomer distribution for $z \leq R_F$ which reads as $\phi(z) = \sigma(z/a)^{0.7}$ ($(1 - \nu)/\nu = 0.7$). For $R > R_F$, the asymptotic profile[7] writes as

$$\phi(z) \propto \left(\frac{z}{R_F}\right)^{-1.611} \exp\left[-0.137\left(\frac{z}{R_F}\right)^{2.427}\right] \tag{3}$$

Regarding the end-chain distribution, the same approach provides

$$g(z) \propto \left(\frac{1}{R_e}\right)[z/R_e]^{\eta_{||}-\eta_{\perp}} \exp[-a_2(z/R_e)^{\delta}] \tag{4}$$

where $\eta_{||}$ and $\eta_{\perp}$ are the surface exponents of the ordinary transition with $\eta_{||} - \eta_{\perp} = 0.816$, $a_2 = 1.269$, $\delta = 2.427$ is the des Cloizeaux exponent, and $R_e$ is the end-to-end distance of the chain ($R_e = 2.501R_F$) in good solvent. The normalization of $g(z)$ is obtained by writing that there is one end per chain.

## III. Polymer Synthesis

All glass reactors with break-seals and standard high-vacuum line techniques were used in this work.[18] Styrene (Fisher Scientific) was purified on a vacuum line by stirring overnight over freshly ground calcium hydride (Aldrich) with degassing, distillation over dibutylmagnesium (Aldrich) for several hours (whereby a characteristic yellow color was formed), and distillation into calibrated ampules. Isoprene (Aldrich) was purified by exposure to calcium hydride with degassing, exposure to sodium dispersion for several hours, and exposure to *n*-butyllithium for 20 min at ice bath temperature, followed by distillation into ampules. Anionic polymerization of styrene was initiated by using *sec*-butyllithium as initiator and benzene as solvent. The benzene (Fisher) was purified by treatment with concentrated sulfuric acid, preliminary drying over calcium hydride, drying over sodium dispersion with degassing on the vacuum line, and storage over polystyryllithium oligomers until use. After complete styrene polymerization (36 h), a sample of the living PS was taken and terminated with degassed methanol. To the remainder of the living PS solution, isoprene was added

and allowed to polymerize for 24 h. A sample of the diblock was taken and terminated with degassed methanol. To the remainder of the living diblock copolymer, a 10-fold excess of chlorotrimethylgermanium (Gelest, purified, by distillation on the high-vacuum line taking the middle fraction and diluted with benzene) was added in order to create the Ge end-capped copolymer. The polymer was precipitated into methanol and washed with excess methanol to remove the excess of the chlorotrimethylgermanium. The synthesis is shown schematically as follows:

$$\text{styrene} + \textit{sec}\text{-BuLi} \rightarrow \text{PS}^-\text{Li}^+$$

$$\text{PS}^-\text{Li}^+ + \text{isoprene} \rightarrow \text{PS}-\text{PI}^-\text{Li}^+$$

$$\text{PS}-\text{PI}^-\text{Li}^+ + (\text{CH}_3)_3\text{GeCl (excess)} \rightarrow \text{PS}-\text{PI}-\text{Ge}(\text{CH}_3)_3$$

Analysis of the molecular weights of the copolymer segments was carried out using a Waters GPC (model 515 pump, model 410 differential refractometer, and two linear Ultrastyragel columns in series) operating in tetrahydrofuran. The GPC system was calibrated using narrow molecular weight distribution PS and PI standards. The number-average degrees of polymerization of the PS and PI segments are respectively 83 (8.6K) and 1706 (116K), with a polydispersity ratio for the diblock of 1.05. Proton NMR measurements using a Bruker 400 MHz instrument were used to confirm composition (6.9 and 93.1 wt % for PS and PI, respectively, in good agreement with the monomer weights that were charged).

## IV. Preparation of Polymer Layers on Silicon Substrates

**A. Pressure−Area Isotherms of the Copolymer Monolayer**. Although diblock copolymers may adsorb on solid substrates from a selective solvent for one block, this simple adsorption does not provide the highest possible density. Hence, an horizontal variation of the Langmuir-Schaeffer technique was used to form condensed monolayers of the diblock copolymer which were eventually transferred to a solid substrate.[19] The monolayers were spread from a 1 g/L solution of PSPIGe in toluene on a Langmuir trough (Riegler−Kirstein) filled with deionized water (Millipore, resistivity higher than 18 MΩ·cm) at 25 °C. Toluene is an equally good solvent for both polystyrene and polyisoprene, and hence micelle or aggregate formation in solution can be ruled out. Since both isoprene and styrene are insoluble in water, it is also unlikely that loss of material takes place inside water due to micelle or vesicle formation. After spreading of the PSPIGe solution, we waited for about 30 min to allow for evaporation of toluene and equilibration of the copolymer. The monolayer was compressed using symmetric barriers of the trough. Typical $\pi-A$ isotherms are shown in Figure 1 in three different pieces because of the finite compression ratio of our trough. It resembles that of a long chain polymer,[20] which could be expected since the diblock copolymer is highly asymmetric with the polystyrene component being less than 10 wt %, and hence the isotherm is expected to be dominated by the polyisoprene component. Since the surface tension of polyisoprene is lower than polystyrene, it is expected that the former would be closer to air. In order to better characterize the in-plane organization of the polymer layer before transfer on the Si wafer, several Brewster angle microscopy (BAM) images (Figure 2) were taken at various areas per molecule (see the corresponding arrows in Figure 1).

Such pictures are only focused on a central stripe because of the projection geometry of the setup. Starting from a 1 g/L solution, 200 $\mu$L of solution is spread, resulting in a negligible surface pressure for an area per molecule of ∼1000 Å$^2$ per chain. The image of Figure 2a is then obtained where large dark sectors coexist with clearer zones of denser polymer. As shown in Figure 1, the pressure is close to zero in this region, which is consistent with the observation of isolated bright polymer domains in Figure 2a.

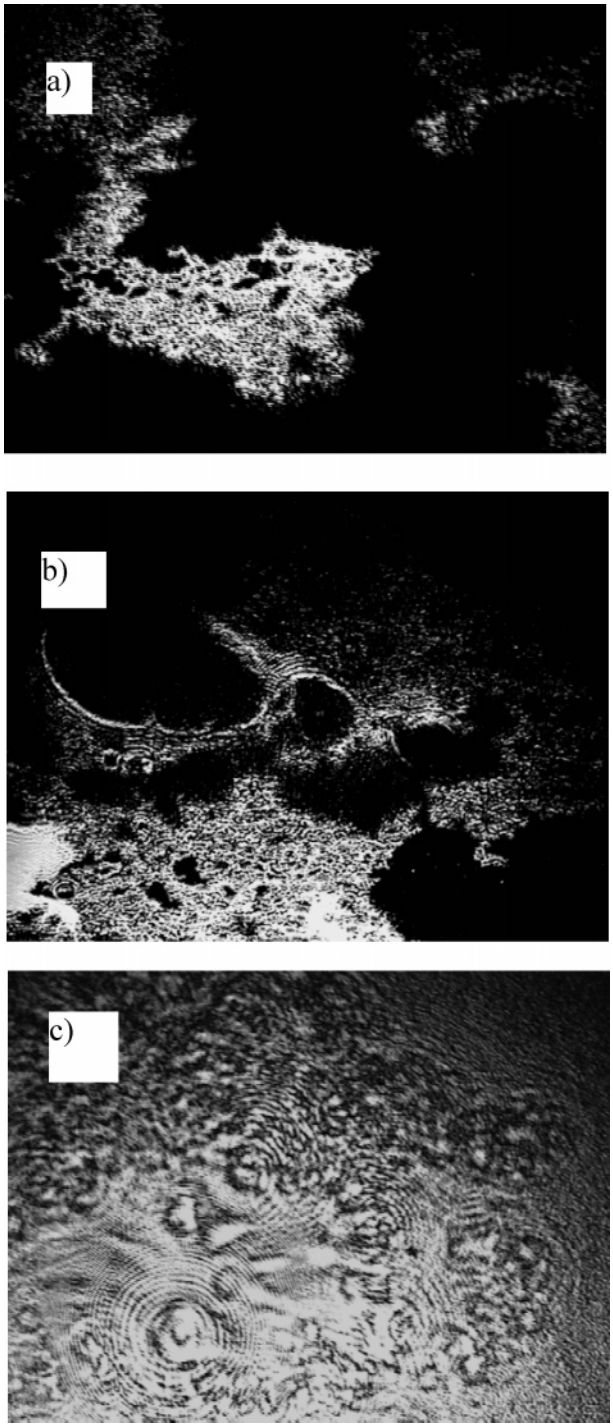


**Figure 2.** BAM pictures showing the layer morphology at different pressures and molecular areas indicated by arrows in Figure 1: (a) $\Pi = 0$ mN/m, (b) $\Pi = 3$ mN/m, and (c) $\Pi = 14$ mN/m. 3D domains are visible in (c).

Upon further compression, the domains become connected and the pressure increases. In order to make dense polymer layers, more polymer (100 $\mu$L) had to be added. This was done after decompression when the pressure was back to zero. Further compression enabled the pressure to increase to 3 mN/m

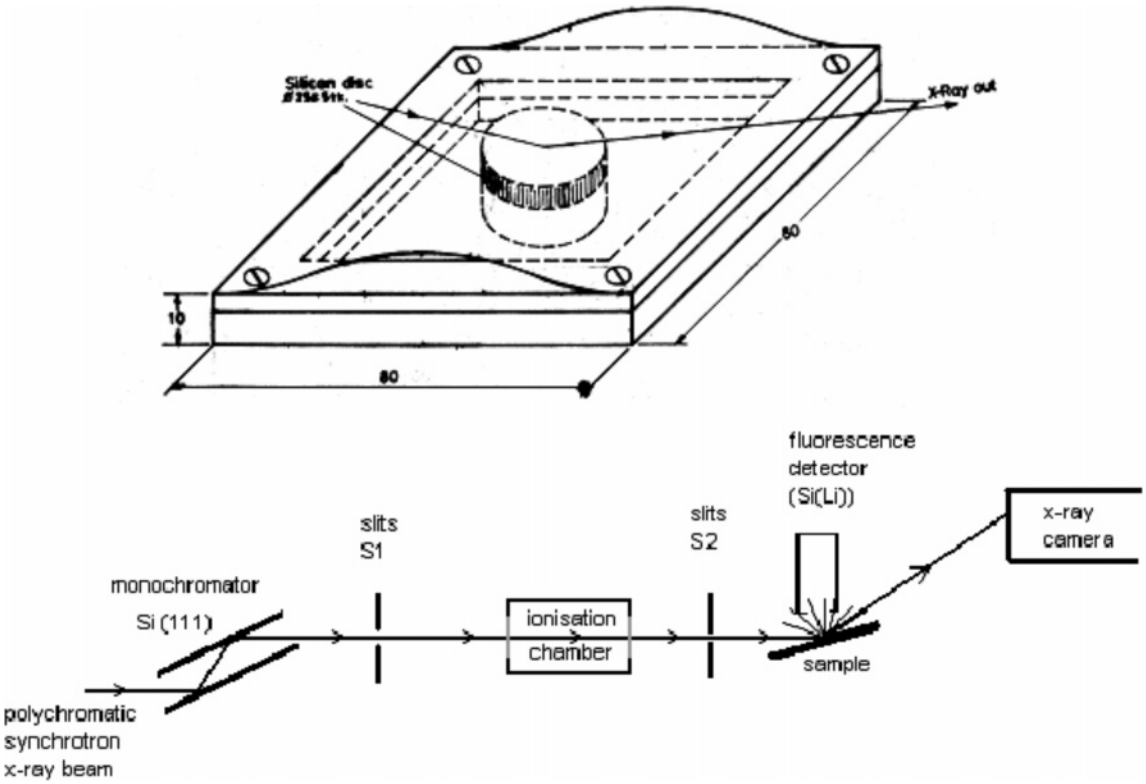


**Figure 3.** Top: scheme of the experimental cell with all dimensions in millimeters. Bottom: scheme of the X-ray beamline at LURE.

where Figure 2b was taken. In this figure, the brighter region in the left lower corner is a 3D domain thicker than a monolayer. Letting the layer relax at this area overnight (Figure 1) made the pressure increase with time. We suggest that this is due to partial spreading of the 3D polymer domains in the monolayer voids. Further addition (100 $\mu$L) leads to Figure 2c at the end of the compression with more 3D polymer domains.

At this point, Brewster images tend to indicate that the transferred polymer layer is a dense rough structure on the picture scale (of order 500 $\mu$m on the horizontal direction).

**C. Transfer and Consolidation of the Layer.** Deposition of the spread monolayer onto solid wafers was performed by placing the substrate below the surface prior to spreading of PSPIGe and pulling it out slowly at the designated pressure, parallel to the surface. A cycle of compression, just before collapse, followed by decompression was followed to ensure formation of a compact monolayer by driving out voids. The Langmuir-Schaeffer transfer was made in the second compression at pressures of 50 mN/m, which was held constant during deposition. The substrates used were silicon wafers spin-coated with 100 Å thick polystyrene films (of $M_w$ = 100K) and annealed at 150 °C for 12 h. The deposited layer was then annealed at 150 °C for 30 min to drive out adsorbed water and to ensure that the styrene segments of the diblock copolymer diffuse into the styrene layer on Si substrate.[19] On cooling below glass temperature, the diblock copolymer becomes irreversibly attached to the substrate, thus reducing the possibility of loss of the diblock copolymer in the solvent. However, when considering the surface densities (see below), it is very likely that many chains desorb into solution.

The roughness inferred from BAM is confirmed by AFM measurements (of order 5−6 nm rms) on layers transferred to substrates. Since measurements of X-ray reflectivity on polystyrene-coated silicon substrates indicate a very small roughness of ∼1−2 nm, which is typical of such films, this means that the roughness primarily comes from the incomplete coverage of the flat pancake-like mushrooms (with very low roughness) and the intervening voids.

## V. X-ray Standing Wave Experiments

**A. Principles**. GIXSWF is a high-resolution technique able to obtain elemental profiles of materials across buried and multilayer interfaces.[21,22,23] The standing waves are formed due to the interference between transmitted and reflected electric fields generated in a medium due to incident X-rays of a given energy. For a given incident energy the standing wave period can be varied by changing the angle of incident X-rays. An atomic species in a fixed location is thus subjected to the electric field which can then excite a suitable fluorescence line. Since the electric field passes through maxima and minima at a given location, $z$, from the surface, the emitted fluorescence from that particular location varies with the angle. However, in a typical measurement what is collected by a suitable energy-dispersive detector is the integrated fluorescence coming from the entire sample at a given angle. The fluorescence intensity profile as a function of incident angle of the X-ray beam can then be modeled to obtain the density profile of only the particular atomic species whose fluorescence emission has been collected. This is in contrast to techniques like X-ray and neutron reflectivity where one obtains the density profile averaged over all atomic species present in the material. The analysis of X-ray standing wave data requires to model the electric field across the sample $E(z)$. The fluorescence intensity is then

$$I \propto \int \mathrm{d}z\, g(z)|E(z)|^2 \tag{5}$$

where $g(z)$ is the density of fluorescent Ge atoms, here the end-segment density. $E(z)$ is calculated using a classical recursive method,[24,25] where the electron density profile is decomposed in slabs of constant refractive index.

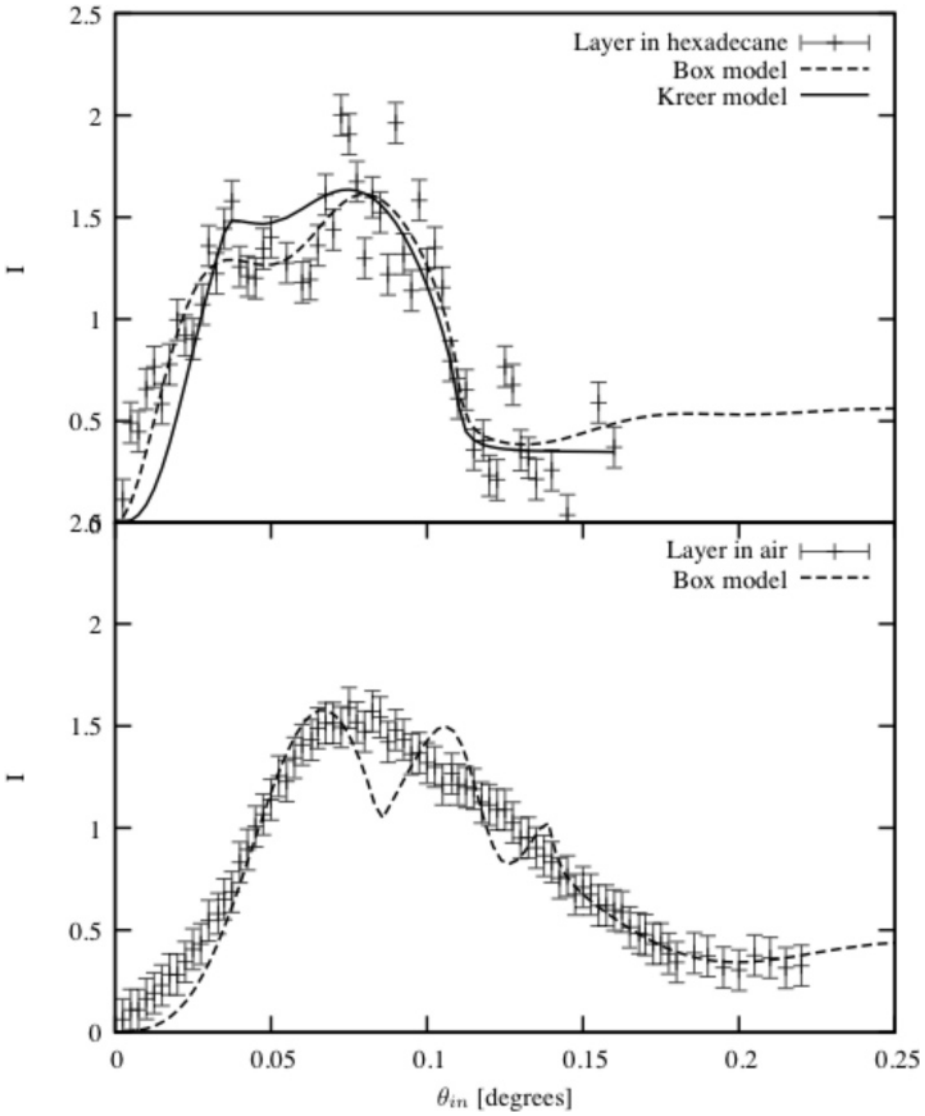


**Figure 4.** Experimental X-ray standing wave data (points) of fluorescence intensity (a.u.) vs the angle of incidence and best fits using the Kreer model (solid line) or box model (dashed line) as described in the text. Bottom: layer in air; top: layer in hexadecane.

**B. Fluorescence Measurements.** GIXSWF measurements were performed at beamline D25 in LURE. The energy of the incident beam was tuned to 12.795 keV using a double bounce Si(111) monochromator. Measurements were made in a custom-designed cell, with and without hexadecane. The Ge Kα (9.886 keV) fluorescence was detected using a Si(Li) detector placed normal to the surface of the substrate, at a distance of 5 mm from it, while the reflected beam was monitored using an X-ray camera and scintillation detector (not shown in Figure 3). The incident beam was collimated using a $5 \times 2000$ $\mu$m slit just before the sample stage.

The intensities of the integrated fluorescence peaks of Ge are plotted in bottom and top parts of Figure 4 as a function of the grazing angle of incidence for both cases of the dry and solvated chains, respectively. The difference in location of the maxima clearly indicates qualitatively that the solvated chains are swollen in contrast to the dry chains, as expected. The biggest challenge for this experiment is to measure a sufficient signal over noise ratio from the tethered chains in solvent. The signal is reduced by several orders of magnitude due to two factors: strong absorption of incident and fluorescent beam in the liquid and considerable reduction of in-plane density of Ge atoms due to the stretching of the end-tethered chains in good solvent.

**C. Data Analysis.** Since the electron densities of polystyrene, polyisoprene, and hexadecane are almost identical, the electric field for the end-tethered chains in hexadecane could be simply modeled using a single electron density slab for the polystyrene film and the end-attached chains in between silicon (refractive index $n = 1-(2.94e^{-6})$ and hexadecane ($n = 1-(1.12e^{-6})$. The fit of the dry chains in air was more difficult because the adsorbed layer is rough (see Figure 4). This is much less in hexadecane, as mentioned above, and in that case there is no roughness perturbing neither the measurement nor the analysis since there is no contrast and no perturbation of the electric field profile (Figure 5). In the dry case, if one does not take roughness into account, no satisfactory agreement can be obtained, since in particular the maximum of the fluorescence is shifted to the left of the critical angle for total external reflection $\theta_c = (2 \times 1.29 \times 10^{-6})^{1/2} = 0.092°$. A better agreement can be obtained following ref 26 where a perturbation theory (second-order distorted-wave Born approximation) was developed to take the roughness into account. Considering only the air−polymer interface below the critical angle for total external reflection, the fluorescence signal without roughness would be proportional to $k'_1/k_0 \mid t \mid^2$ where $k_0$ is the normal component of the wavevector in air, $k'_1$ is the real part of the vertical component of the wavevector in the polymer and $t$ is

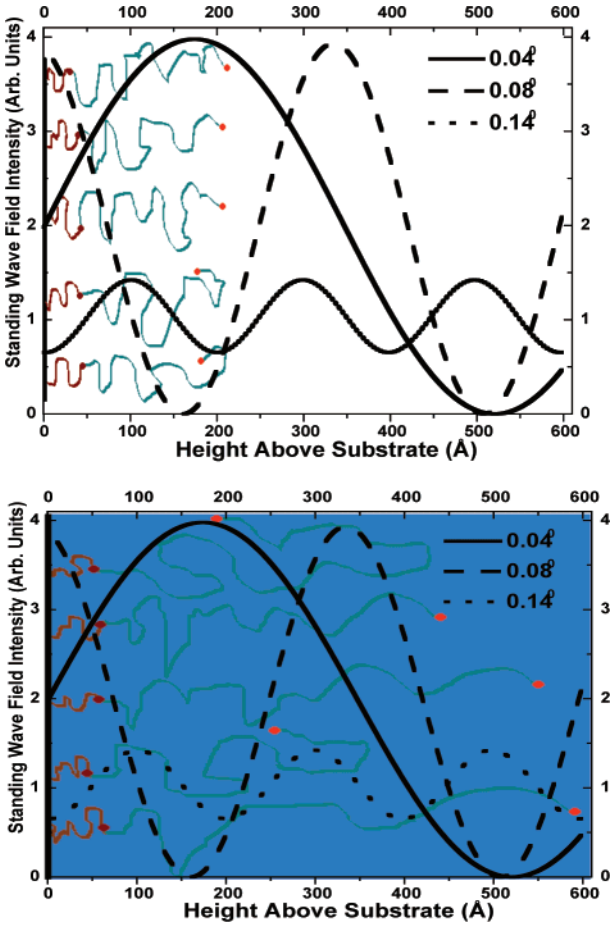


**Figure 5.** Top: schematic of copolymer mushroom configuration in air with the standing wave field at different incident angles. Bottom: same as top with the end-tethered chains in good solvent (hexadecane). Junction points between PS and PI are the dark spheres, and the end-groups of Ge are the light spheres. Note that for clarity the Ge atoms trapped at the PS surface are not shown.

the transmission coefficient at the air−polymer interface. The main contribution from the roughness is the absorption factor in the rough interfacial layer: $2k'_1/k_0|t|^2k''_1{}^2\sigma^2$, where $k''_1$ is the imaginary part of the normal component of the wavevector in the polymer and $\sigma$ the rms roughness at the air−polymer interface. As $k''_1$ is much larger below the critical angle for total external reflection than above it, the main effect is to shift the fluorescence curve toward lower grazing angles of incidence. This accounts for our observation though due to our high estimated roughness (7 nm) we probably have to push the approximation to the limit. This value is however consistent with AFM measurements which indicate a roughness of 5−6 nm. It is clear from AFM images that this roughness arises due to low-density heterogeneous domains of roughly constant height with voids in between indicating a mushroom configuration of chains, as explained later in the Discussion.

## VI. Discussion

First, in order to perform a model-independent analysis, we divided the sample into slabs of constant density. The number of slabs was systematically varied in order to determine the minimum number of slabs necessary to fit our data (Figure 6). Adding too many slabs increases the number of fitting parameters and therefore increases the value of $\chi^2$ though the fit quality is not improved. The extension of the chains is much larger in good solvent compared to the dry layer, and it is also remarkable that the profile in good solvent is continuous (end-segments are found at any distance from the surface) whereas the dry profile is singular. Moreover, a significant part of the end-segments are trapped at the surface in both cases. We will address this issue in the following.

The Flory radius of the PI chain can be estimated from correlations[27] established for PI in cyclohexane and giving $R_F = 1.26 \times 10^{-2}M^{0.610}$, which leads to $R_F \sim 15.5$ nm. Since the measured thickness is only $\sim 3R_F$, we decided to also analyze our data using the Kreer et al. theory[7] (plus a distribution of end-segments localized at the surface) which applies for the end-segment distribution of mushrooms. As can be seen in Figure 4, the agreement between the model-independent analysis and the analytical profile fitting is very satisfactory. In particular, the layer extension in hexadecane is found to be the same using both methods as seen in Figure 6, supporting our mushroom analysis. The agreement is also very good concerning the profile shape. Whereas the model-independent analysis only comprises three slabs, it yields a continuous distribution of end-segments with a maximum in the middle, matching well the Kreer et al. profile. In agreement with the latter, it is remarkable that the end-segment profiles extends up to $\sim 3R_F = 45$ nm. This confirms that the layer is not dense enough to be a brush since with $D \sim R_F$, formula 2 predicts an extension of order 160 nm, much higher than our experimental findings. It has been checked

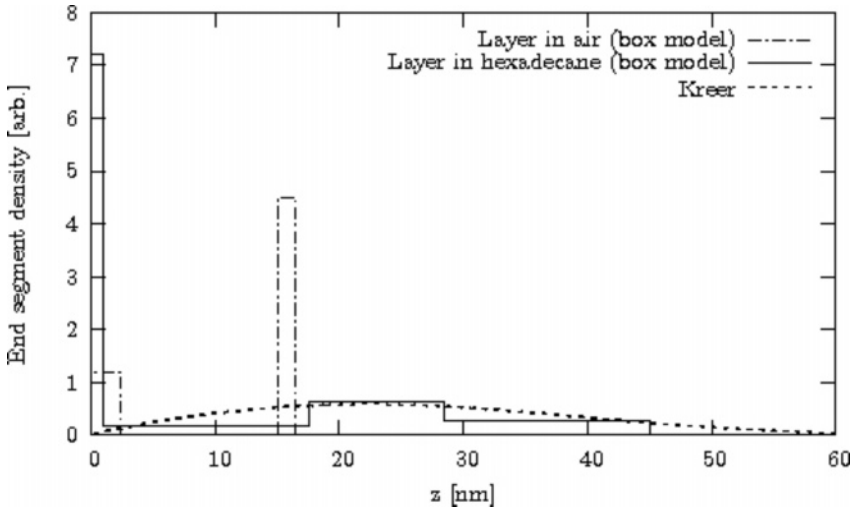


**Figure 6.** End-segment density profiles resulting from the fits of the experimental data. Dashed-dotted line: box model for the layer in air; solid line: box model for the layer in hexadecane; dotted model: Kreer model for the layer in hexadecane.

that taking into account the chain polydispersity does not modify this analysis since the Kreer function for the average end-to end distance nicely matches the weighted average of the Kreer functions for different end-to-end distances.

In air, in the absence of available analytical formula for dry mushrooms, we only analyzed our data with the slab model. It is remarkable that the profile (see Figure 6) is reminiscent of the Alexander−de Gennes approximation (all chains ending at the extremity of the layer). At this low density in a bad solvent, it is reasonable to expect the layer to collapse in heterogeneous domains, as confirmed by AFM measurements. Following the analysis of Lyulin et al.[28] where the end-segments are shown to segregate at the surface of the domains for entropic reasons, one may understand why end-segments are mostly located at the external surface of PI pancakes collapsed on top of the PS layer.

Let us finally come back to the localization of the end-segments onto the polystyrene-coated silicon surface. We estimated the strength of the van der Waals interaction between germanium and polystyrene interacting across air and hexadecane. The Hamaker constant for germanium−air−polystyrene system estimated using the data of ref 29 and the combination rules of ref 30 is $\sim 35 k_B T$. The van der Waals interaction energy, $W$, is given by $W = -Ar/6d$ with $A$ the effective Hamaker constant for the germanium−medium−substrate system, $r$ the Ge atom radius, and $d$ the distance between the Ge atom and the surface. Assuming $r = 1.22 \times 10^{-10}$ m, the van der Waals interaction strength is of order $2k_B T$ at a distance $d$ of 0.2 nm in air. This explains why some Ge atoms may partition to the outer fringe of the PS surface during annealing as detected by X-ray fluorescence (see above) where they can be irreversibly trapped. For germanium interacting across hexadecane with polystyrene, using the values of Hamaker constants provided in refs 29 and ref 30, the Hamaker constant is $\sim 3 k_B T$, and the van der Waals interaction across a distance of 0.2 nm amounts to $\sim 0.15 k_B T$. This value is significantly smaller than the van der Waals interaction in air. Since there are some discrepancies in the Hamaker constants of hexadecane and polystyrene (the two values might be very close), we have also looked at an alternative scenario by calculating van der Waals interaction between germanium and silicon across an effective organic medium (hexadecane + polystyrene). In this case we find that the Hamaker constant is larger, $\sim 25 k_B T$, consistent with the experimental value of $50 k_B T$ for gold−tetradecane−gold.[30] However, in this case the interaction takes place across a distance of ~10 nm (thickness of coated polystyrene film) which leads to van der Waals interaction energy of $\sim 0.05 k_B T$, which is even more insignificant. Hence, from all these considerations the sticking probability of germanium on polystyrene is considerably smaller than in air. We then rule out any specific adsorption of the Ge which remained free after annealing. Since trapped Ge atoms are localized at the very surface of the PS film, and PS and PI segments are incompatible, no mixing of PS and PI is expected: all chains with a free end are thus expected to have the same nominal length.

## VII. Conclusion

To our knowledge, we have presented the first available data of a direct measurement of the end-segment distribution of polymer layers in-situ in different conformations using X-ray standing waves. Our results show the sensitivity of the method to measure very small amounts of matter (well below one atom per 100 Å$^2$ on average), even in a liquid environment, and this method could be used in many other polymer studies. We find a quantitative agreement with the renormalization group calculations (Kreer et al. profile). A very different singular profile is found in a bad solvent, as qualitatively expected.

**Acknowledgment.** J.D. and J.K.B. gratefully acknowledge support from the Indo-French Center for Advanced Research under Grant #2504-2. J.D., J.K.B., and P.G. thank C. M. Marques and A. Johner for useful discussions on the end-chain distribution of mushrooms. J.W.M. acknowledges support by the Division of Chemical Sciences, Geosciences, and Biosciences, Office of Basic Energy Science, U.S. Department of Energy, under Contract DE-AC05-00OR22725 with Oak Ridge National Laboratory, managed and operated by UT-Battelle, LLC.

## References and Notes

(1) Fleer, G. J.; Cohen Stuart, M. A.; Scheutjens, J. M. H. M.; Cosgrove, T.; Vincent, B. *Polymers at Interfaces*; Chapman & Hall: London, 1993. Halperin, A.; Tirrell, M.; Lodge, T. P. *Adv. Polym. Sci.* **1992**, *100*, 31.
(2) Brochard, F.; de Gennes, P. G. *Langmuir* **1992**, *8*, 1033.
(3) Alexander, S. *J. Phys. (Paris)* **1977**, *38*, 983.
(4) de Gennes, P. G. *Macromolecules* **1980**, *13*, 1069.
(5) Milner, S. T.; Witten, T. A.; Cates, M. E. *Europhys. Lett.* **1988**, *5*, 413.
(6) de Gennes, P. G. *Adv. Colloid Interface Sci.* **1987**, *27*, 189.
(7) Kreer, T.; Metzger, S.; Müller, M.; Binder, K.; Baschnagel, J. *J. Chem. Phys.* **2004**, *120*, 4012.
(8) Auroy, P.; Auvray, L.; Léger, L. *Macromolecules* **1991**, *34*, 2523.
(9) Romet-Lemonne, G.; Daillant, J.; Guenoun, P.; Yang, J.; Mays, J. W. *Phys. Rev. Lett.* **2004**, *93*, 148301.
(10) Zhao, B.; Brittain, W. J. *Prog. Polym. Sci.* **2000**, *25*, 677.
(11) Ansarifar, M. A.; Luckham, P. F. *Polymer* **1988**, *29*, 329. Marra, J.; Hair, M. L. *Colloids Surf.* **1988**, *34*, 215.
(12) Brandrup, J., Immergut, E. H., Grulke, E. A., Eds.; *Polymer Handbook*; Wiley-Interscience: New York, 1999; Vol. 1−2.
(13) Cosgrove, T.; Heath, T.; Van Lent, B.; Leermakers, F.; Scheutjens, J. M. H. M. *Macromolecules* **1987**, *20*, 1692.
(14) Zhulina, E. B.; Borisov, O. V.; Priamytsin, V. A. *J. Colloid Interface Sci.* **1990**, *137*, 495.
(15) Semenov, A. N. *Sov. Phys. JETP* **1985**, *61*, 733.
(16) Zhulina, E. B.; Borisov, O. V.; Priamitsyn, V. A.; Birshtein, T. M. *Macromolecules* **1991**, *24*, 140.
(17) de Gennes, P. G. *Macromolecules* **1980**, *13*, 1069.
(18) Uhrig, D.; Mays, J. W. *J. Polym. Sci., Part A: Polym. Chem.* **2005**, *43*, 6179.
(19) Currie, E. P. K.; Sieval, A. B.; Avena, M.; Zuilhof, H.; Sudholter, E. J. R.; Cohen Stuart, M. A. *Langmuir* **1999**, *15*, 7116.
(20) Heger, R.; Goedel, W. A. *Macromolecules* **1996**, *29*, 8912.
(21) Bedzyk, M. J.; Bommarito, G. M.; Caffrey, M.; Penner, T. L. *Science* **1990**, *248*, 52.
(22) Wang, J.; Caffrey, M.; Bedzyk, M. J.; Penner, T. L. *Langmuir* **2001**, *17*, 3671.
(23) Fenter, P.; Cheng, L.; Rihs, E.; Machewsky, M.; Bedzyk, M. J.; Sturchio, N. C. *J. Colloid Interface Sci.* **2000**, *225*, 154.
(24) Herpin, A. *C. R. Acad. Sci. Paris* **1947**, *225*, 182.
(25) *X-ray and Neutron Reflectivity: Principles and Applications*; Daillant, J., Gibaud, A., Eds.; Springer: Berlin, 1999.
(26) de Boer, D. K. G. *Phys. Rev. B* **1996**, *51*, 5297.
(27) Fetters, L. J.; Hadjichristidis, N.; Lindner, J. S.; Mays, J. W. *J. Phys. Chem. Ref. Data* **1994**, *23* (4), 619−640.
(28) Lyulin, A. V.; Dünweg, B.; Borisov, O. V.; Darinskii, A. A. *Macromolecules* **1999**, *32*, 3264.
(29) Visser, J. *Adv. Colloid Interface Sci.* **1972**, *3*, 331.
(30) Lyklema, H. *Fundamentals of Interface and Colloid Science*, 2nd ed.; Academic Press: New York, 1993; Vol. 1.

MA070817D